REVIEW SUMMARY

QUANTUM MATERIALS

Polaritons in van der Waals materials

D. N. Basov,* M. M. Fogler, F. J. García de Abajo

BACKGROUND: Light trapped at the nanoscale, deep below the optical wavelength, exhibits an increase in the associated electric field strength, which results in enhanced light-matter interaction. This leads to strong nonlinearities, large photonic forces, and enhanced emission and absorption probabilities. A practical approach toward nanoscale light trapping and manipulation is offered by interfaces separating media with permittivities of opposite signs. Such interfaces sustain hybrid light-matter modes involving collective oscillations of polarization charges in matter, hence the term polaritons. Surface plasmon polaritons, supported by electrons in metals, constitute a most-studied prominent example. Yet there are many other varieties of polaritons, including those formed by atomic vibrations in polar insulators, excitons in semiconductors, Cooper pairs in superconductors, and spin resonances in (anti) ferromagnets. Together, they span a broad region of the electromagnetic spectrum, ranging from microwave to ultraviolet wavelengths. We discuss polaritons in van der Waals (vdW) materials: layered systems in which individual atomic planes are bonded by weak vdW attraction (see the figure). This class of quantum materials includes graphene and other two-dimensional crystals. In artificial structures assembled from dissimilar vdW atomic layers, polaritons associated with different constituents can interact to produce unique optical effects by design.

ADVANCES: vdW materials host a full suite of different polaritonic modes with the highest degree of confinement among all known materials. Advanced near-field imaging methods allow the polaritonic waves to be launched and visualized as they travel along vdW layers or through multilayered heterostructures. Spectroscopic and nano-imaging experiments have identified multiple routes toward manipulation of nano-optical phenomena endowed by polaritons. A virtue of polaritons in vdW systems is their electrical tunability. Furthermore, in heterostructures assembled from dissimilar vdW layers, different brands of polaritons interact with each other, thus enabling unparalleled control of polaritonic response at the level of single atomic planes. New optoelectronic device concepts aimed at the detection, harvesting, emission, propagation, and modulation of light are becoming feasible as a result of combined synthesis, nanofabrication, and modeling of vdW systems. The extreme anisotropy of vdW systems leading to opposite signs of the in-plane and out-of-plane permittivities of the same layered crystal enables efficient polaritonic waveguides, which are instrumental for subdiffractional focusing and imaging. In addition to near-field optical probes facilitating nanoimaging, coupling to polaritons can be accomplished via electrical excitation and nonlinear wave mixing.

OUTLOOK: Potential outcomes of polariton exploration in vdW heterostructures go beyond nano-optical technologies. In particular, images of polaritonic standing and traveling waves contain rich insights into quantum phenomena occurring in the host material supporting polaritons. This line of inquiry into fundamental physics through polaritonic observations constitutes an approach toward optics-based materials research. In particular, the strong spatial confinement exhibited by vdW polaritons involves large optical-field gradients—or equivalently, large momenta—which allows regions of the dispersion relations of electrons, phonons, and other condensed-matter excitations to be accessed beyond what is currently possible with conventional optics. Additionally, polaritons created by short and intense laser pulses add femtosecond resolution to the study of these phenomena. Alongside future advances in the understanding of the physics and interactions of vdW polaritons, solutions to application challenges may be anticipated in areas such as loss compensation, nanoscale lasing, quantum optics, and nanomanipulation. The field of vdW polaritonics is ripe for exploring genuinely unique physical scenarios and exploiting these new phenomena in technology. ∎

ON OUR WEBSITE

Read the full article at http://dx.doi.org/10.1126/science.aag1992
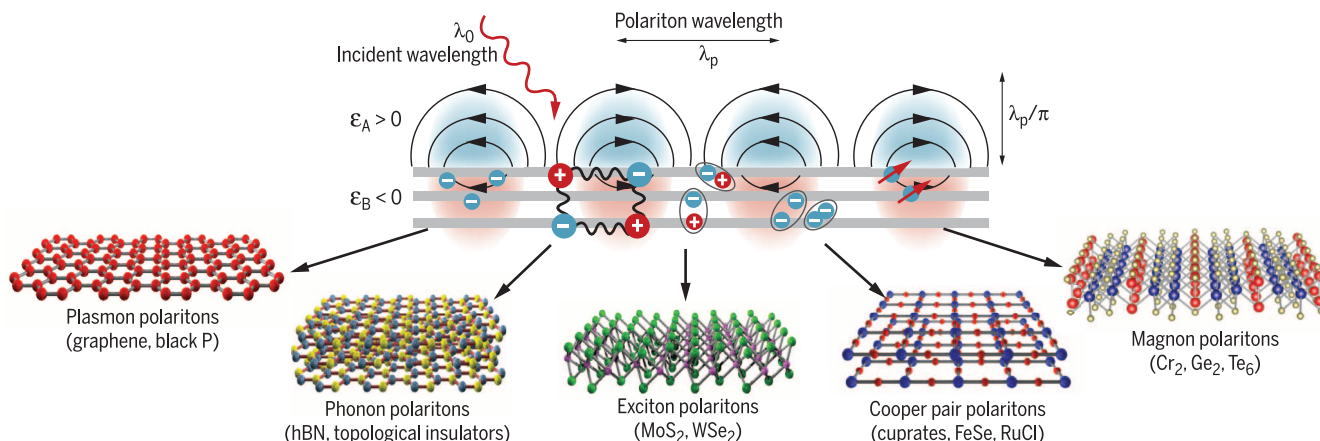
Polaritons in van der Waals (vdW) materials. Polaritons—a hybrid of light-matter oscillations—can originate in different physical phenomena: conduction electrons in graphene and topological insulators (surface plasmon polaritons), infrared-active phonons in boron nitride (phonon polaritons), excitons in dichalcogenide materials (exciton polaritons), superfluidity in FeSe- and Cu-based superconductors with high critical temperature T_c (Cooper-pair polaritons), and magnetic resonances (magnon polaritons). The family of vdW materials supports all of these polaritons. The matter oscillation component results in negative permittivity ($\varepsilon_B < 0$) of the polaritonic material, giving rise to optical-field confinement at the interface with a positive-permittivity ($\varepsilon_A > 0$) environment. vdW polaritons exhibit strong confinement, as defined by the ratio of incident light wavelength λ_O to polariton wavelength λ_p.

REVIEW

QUANTUM MATERIALS

Polaritons in van der Waals materials

D. N. Basov,[1,2]* M. M. Fogler,[1] F. J. García de Abajo[3,4]

van der Waals (vdW) materials consist of individual atomic planes bonded by weak vdW attraction. They display nearly all optical phenomena found in solids, including plasmonic oscillations of free electrons characteristic of metals, light emission/lasing and excitons encountered in semiconductors, and intense phonon resonances typical of insulators. These phenomena are embodied in confined light-matter hybrid modes termed polaritons—excitations of polarizable media, which are classified according to the origin of the polarization. The most studied varieties are plasmon, phonon, and exciton polaritons. In vdW materials, polaritons exhibit extraordinary properties that are directly affected by dimensionality and topology, as revealed by state-of-the-art imaging of polaritonic waves. vdW heterostructures provide unprecedented control over the polaritonic response, enabling new quantum phenomena and nanophotonics applications.

Atomically thin two-dimensional (2D) crystalline layers constitute the elemental building blocks of van der Waals (vdW) materials. Exfoliated atomic layers are structurally robust and amenable to assembly to produce complex heterostructures. These materials support a variety of polaritons associated with oscillations of conduction electrons, phonons, and excitons, as well as their hybrids (e.g., plasmon-phonon polaritons). A number of vdW materials display extraordinary quantum phenomena: high–critical temperature (T_c) superconductivity, exotic magnetism, topologically protected states, strong Coulomb interactions, and non–Fermi-liquid behavior. All of these properties permeate the polaritonic response of vdW systems.

In the ongoing quest for exploration of polaritons, scanning optical near-field imaging (Fig. 1) has had an exceptional impact. This technique uses the sharp tip of an atomic force microscope (AFM) as an optical antenna (1, 2), allowing one to detect how incident light of free-space wavelength λ_o is scattered at the apex of the tip in the proximity of the studied specimen (Fig. 1A). The obtained signal is governed by the local electric field of the polariton wave launched by the tip, rendering nanometer spatial resolution as the tip is raster-scanned over the sample. The principal characteristics of polaritons, including wavelength λ_p, confinement ratio λ_o/λ_p, and quality factor Q (Table 1), reveal that vdW polaritons are simultaneously compact and long-lived. The polariton wavelength can often be tuned with various methods, of which electrical gating is of paramount importance. These characteristics render vdW polaritons comple-

mentary and sometimes superior to those observed in more conventional materials (3, 4).

A major challenge of polariton imaging and spectroscopy stems from the large momentum mismatch with free-space photons. However, experimentalists are becoming increasingly adept at overcoming this difficulty. Figure 2 displays various coupling schemes. Coherent launchers (Fig. 2, A to C) have relatively small coupling cross sections, although they can be enhanced through optical antennas, including AFM tips (Fig. 2C) and metal bars or disks (5). Incoherent launchers (Fig. 2, D to F) can reach order-unity efficiency; in particular, electron beams (Fig. 2D) eventually will enable an impressive combination of energy and space resolution (6).

Primer on polaritons

Polariton dispersion in thin layers

When the sample thickness d is much smaller than the wavelength λ_p of polaritons, only the in-plane optical response of the material is important. In this thin-film limit, one finds

$$\lambda_p = \frac{2\pi}{k_p} = 4\pi^2 \, \text{Im}\left\{\frac{\sigma}{\omega\varepsilon_a}\right\}, \; d << \lambda_p \quad (1)$$

where ε_a is the permittivity of the environment, σ is the in-plane conductivity, ω is the frequency, and k_p is the in-plane polariton wave vector. The field of the polariton wave decreases exponentially away from the interface over a characteristic distance $\sim \lambda_p/2\pi$. It is common to describe σ in Eq. 1 as the sum

$$\sigma(\omega) = \frac{i}{\pi}\frac{S_f}{\omega + i\tau_f^{-1}} + \frac{i}{\pi}\frac{\omega S_b}{\omega^2 - \omega_b^2 + i\omega\tau_f^{-1}} \quad (2)$$

The first (Drude) and the second (Lorentz) terms represent the contribution of free (f) and bound (b) charges, respectively. The latter can also account for optical phonons. Different vdW mate-

rials can be modeled with a suitable choice of parameters in Eq. 2: the spectral weights S_f and S_b, the exciton/phonon frequency ω_b, and the phenomenological relaxation times τ_f and τ_b (related to Q in Table 1 by $\tau = Q/\omega$).

The spectral weights in Eq. 2, and therefore the polariton wavelengths of vdW materials, are often tunable. In graphene, S_f scales with the Fermi energy E_F according to $S_f \sim (e/\hbar)^2 E_F$ (where e is the charge on the electron and $\hbar$ is the Planck constant divided by 2π) (7); the value of S_f can be controlled via electrical gating, doping, and photo-excitation. In insulators, where $S_b \sim (e^2/\hbar)f\omega_b$, the dimensionless parameter f scales linearly with the number N of atomic layers. In particular, $f_{ph} \sim N\sqrt{m/M} << 1$ for optical phonons and $f_{ex} \sim N(D/ea_{ex})^2$ for excitons. Here, m, M, a_{ex}, and D are the electron mass, the atomic mass, the exciton Bohr radius, and the exciton transition dipole, respectively. In superconductors, the total Drude weight is constant but is split between normal- and super-current components, with a relative weight depending on temperature. When applied to graphene, Eqs. 1 and 2 readily explain why the surface plasmon polariton (SPP) confinement ratio $\lambda_o/\lambda_p = (\varepsilon_a/\alpha)(\hbar\omega/2E_F) >> 1$ can be extraordinarily high (8): λ_o/λ_p scales with the inverse of the fine-structure constant $\alpha \approx 1/137$. However, a stronger confinement is accompanied by larger damping rate τ_f^{-1} [which also increases with ω (9, 10)].

Polariton dispersion in slabs and heterostructures

For highly confined polaritons (or thicker samples), the condition $\lambda_p >> d$ may not hold, so the polariton dispersion becomes more intricate (Fig. 3). Both the in- and out-of-plane responses need to be considered, and it is more convenient to use the permittivity tensor, whose in-plane component $\varepsilon_\parallel$ relates to $\sigma(\omega)$ as $\varepsilon_\parallel = 1 + (4\pi i\sigma/\omega d)$, whereas the out-of-plane component $\varepsilon_\perp$ may differ from $\varepsilon_\parallel$ in both magnitude and sign because of the strong anisotropy of vdW materials (Fig. 3, E and F). Additional complications arise if the sample is a heterostructure made of dissimilar vdW materials (metals, insulators, or semiconductors). These more complex dispersions can be dissected into simpler elements (11, 12) as in Fig. 3, A to G.

SPPs are supported by materials that possess mobile charges: metals, doped semiconductors, and superconductors. We find three types of electromagnetic modes in these materials (Fig. 3A): two in the bulk (photon and plasmon) and one confined at the surface (lower curve, representing the TM-polarized SPP). The transverse upper branch also starts at frequency ω_p and disperses upward at higher wave vector k. This behavior results from level repulsion between the photon (dashed line in Fig. 3A) and the zero-frequency (Drude) resonance of the conductor. The high-k SPP is often referred to as a surface plasmon (SP). Its dispersion asymptotically approaches $\omega_{SP} = \omega_p/\sqrt{2}$.

The SPPs at the surfaces of a thin conducting film of thickness $d << c/\omega_p$ split into two branches of opposite symmetry. The lower,

[1]Department of Physics, University of California, San Diego, CA, USA. [2]Department of Physics, Columbia University, New York, NY, USA. [3]Institut de Ciencies Fotoniques, Barcelona Institute of Science and Technology, 08860 Castelldefels (Barcelona), Spain. [4]Institució Catalana de Recerca i Estudis Avançats, 08010 Barcelona, Spain.
*Corresponding author. Email: db3056@columbia.edu

Table 1. Characteristics of polaritons in vdW materials. Tunability methods marked with asterisks indicate already demonstrated results. All experimental entries are obtained under ambient conditions, except for Cooper-pair plasmons at T = 5 K. SPP, surface plasmon polariton; DE, dielectric environment; N/A, not available.

| Polariton types (materials)	Image	Energy range (meV)	λ_p (nm)	max λ_0/λ_p	max Q	Tunability methods	References
Dirac SPP (graphene)	Fig. 1A	<1000	50 to 450	220	40	Gating,* doping,* photoexcitation,* DE*	(10, 20, 21, 100)
Edge SPP (graphene)	Fig. 1B	<1000	50 to 200	200	10	Gating,* doping, photoexcitation, DE*	(64, 65)
One-dimensional SSP (carbon nanotubes)	Fig. 1C	<200		100 to 1000	26	Conducting channels,* DE	(30)
Superlattice SPP (graphene/hBN moiré superlattices)	Fig. 1D	<1000	50 to 250	220	4	Gating, doping,* photoexcitation	(24, 101)
Hyperbolic plasmon-phonon polaritons (graphene/hBN)	Fig. 1E	90 to 110 (type I), 170 to 200 (type II)	630 to 750	37	15	Gating,* doping,* photoexcitation	(18, 60)
Hyperbolic plasmon-phonon polaritons [Bi_2Se_3, $(Bi,Sb)_2Te_3$]	N/A	8 to 20				Gating,* doping,* photoexcitation	(93)
Exciton polariton (WSe_2)	Fig. 1F	1400 to 1600	>300	3	5	Crystal thickness,* DE	(45)
Hyperbolic phonon polariton (h-BN)	Fig. 1G	90 to 110 (type I), 170 to 200 (type II)	200 to 1000	50	200	Crystal thickness,* DE*	(17, 82, 102–104)
Topological SPP: Bi_2Se_3, $(BiSb)_2Te_3$	N/A	<200	7 to 5000	900	3	Gating, doping*	(105, 106)
Cooper-pair and Josephson plasmon polaritons (cuprate high-T_c superconductors)	N/A	<40	9000 to 13,000	3	4	Doping, crystal thickness,* DE*	(89, 90, 107, 108)
Anisotropic SPP (black phosphorus)	N/A	<60 ($k \parallel \Gamma$-X), <40 ($k \parallel \Gamma$-Y)					(109)
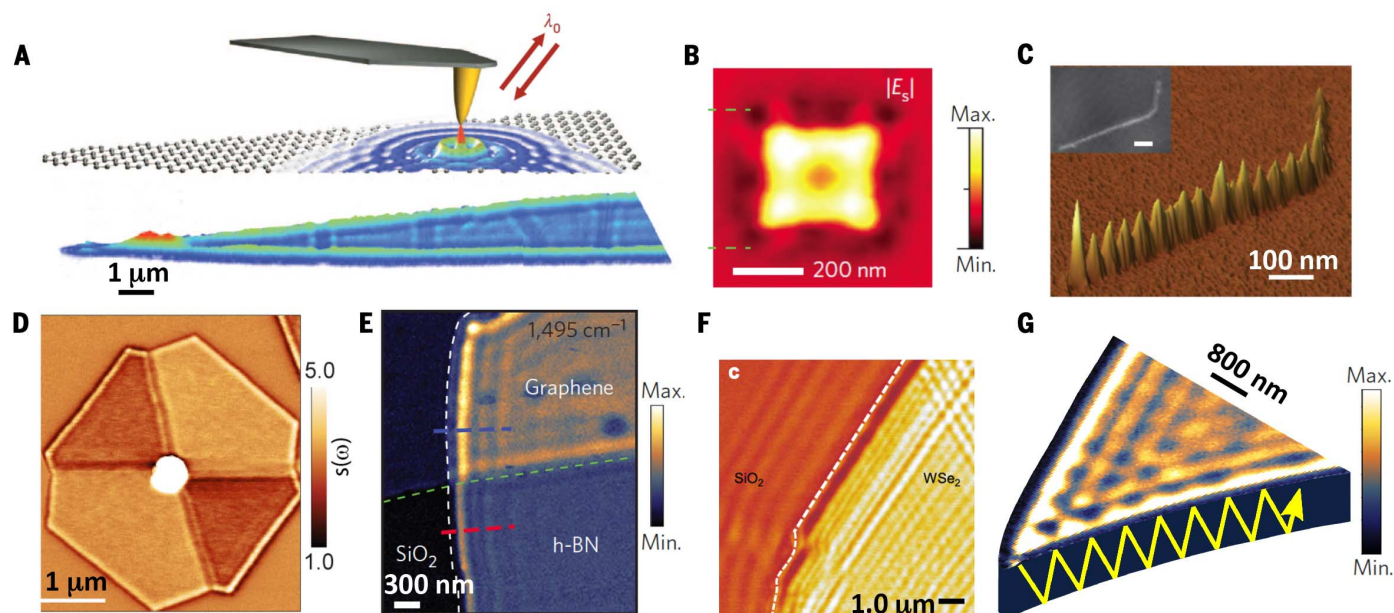
Fig. 1. Polaritons in vdW materials visualized through near-field nanoimaging. (**A**) Dirac plasmons in graphene (20, 21). [Reproduced from (20)] (**B**) Edge plasmons at the boundary of a graphene nanoresonator (64, 65). [Reproduced, with permission, from (65)] (**C**) One-dimensional plasmons in a carbon nanotube (30). [Reproduced, with permission, from (30)] (**D**) Superlattice plasmons in graphene–h-BN moiré superlattices (24). [Reproduced from (24)] (**E**) Hybrid plasmon-phonon polaritons in graphene on h-BN (60). [Reproduced from (60)] (**F**) Exciton polaritons (45) in WSe_2. [Reproduced, with permission, from (45)] (**G**) Hyperbolic phonon polaritons in a h-BN slab (102), propagating as guided waves (schematic line).
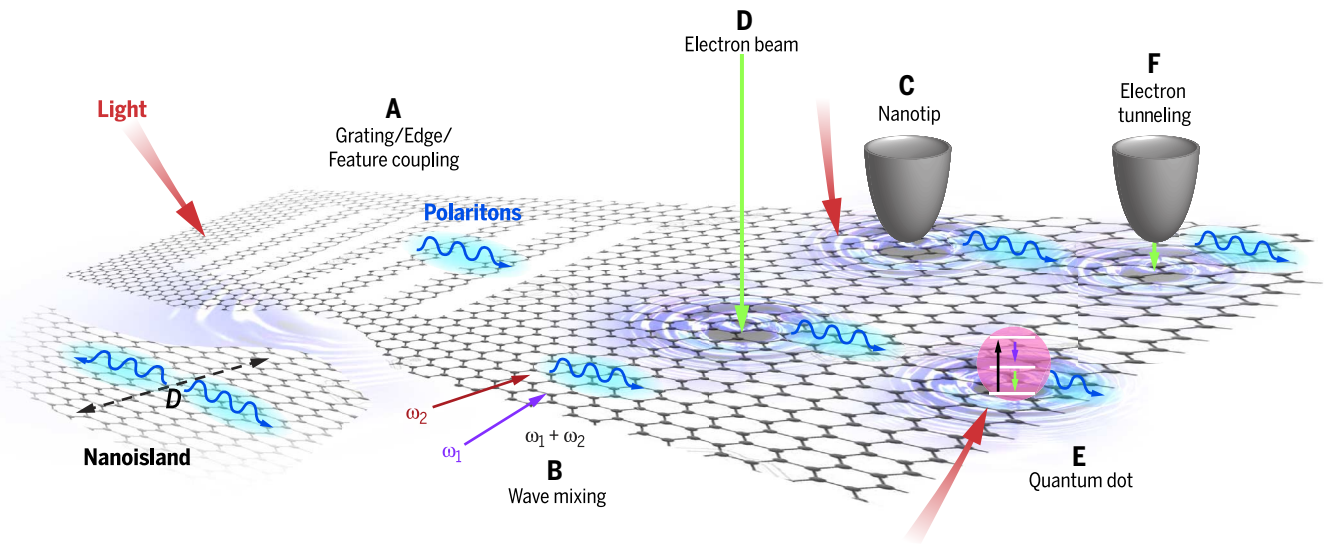
Fig. 2. Launching and visualizing polaritons. (**A** to **F**) Excitation and probing of vdW polaritons (blue arrows) can be achieved using (A) periodic structures (*110–112*), (B) nonlinear wave mixing (*95*), (C) antenna-like nanotips (*20*, *21*), (D) electron beams (*113*), (E) quantum dots and localized emitters (*114*, *115*), and (F) electron tunneling (*116*). Polaritons produced by processes shown in (A) to (C) maintain phase coherence with respect to the external illumination, in contrast to mechanisms shown in (D) to (F), which are inelastic. A variant of (A) has been proposed that relies on surface acoustic wave modulation (*117*, *118*). Sample edges (*64*, *65*) also provide additional momentum to mediate light-polariton coupling. Localized polaritons confined to nanoislands can be resonantly excited by incident light. Radiative outcoupling of polaritons can be visualized by reversing the arrows in (A) to (C).

symmetric branch corresponds to the thin-film plasmons (Eq. 1 and Fig. 3B). For $k \gg 1/d$, both of these branches are localized to the film surfaces and are nearly degenerate. A set of guided waves above the bulk plasmon frequency ω_p may also exist between the light lines of vacuum and the material (tilted dashed lines in Fig. 3B) for films with high-frequency permittivity larger than unity.

Phonon and exciton polaritons in dielectrics

A typical bulk dielectric exhibits three modes: two transverse optical branches of phonon polaritons (PhPs) ω_{TO}, generated by hybridization of a photon (dashed line in Fig. 3C) and a TO phonon; and one longitudinal phonon ω_{LO}, analogous to the bulk plasmon in a metal. In a semi-infinite dielectric, a surface phonon polariton (SPhP) emerges inside the bulk stop band $\omega_{TO} < \omega < \omega_{LO}$. In thin slabs (Fig. 3D), the PhP branches split into guided modes while the SPhP generates symmetric and antisymmetric modes similar to SPPs in metal films. The mode structure of exciton polaritons in semiconductors is similar to that of phonon polaritons in dielectrics, except that the role of ω_{TO} is played by the exciton energy and the dispersion at large momenta is quadratic: $\omega(k) = \omega_{TO} + (\hbar k^2 / 2m_{ex})$, where m_{ex} is the exciton mass. The ω_{LO}-ω_{TO} gap in excitonic systems is referred to as the Rabi splitting.

Hyperbolic media and waveguide modes

Hyperbolic materials exhibit permittivities of opposite signs along different directions. In particular, type II hyperbolic materials possess positive $\varepsilon_\parallel$ and negative $\varepsilon_\perp$. In anisotropic polar dielectrics, this regime may be realized within stop bands. Hyperbolicity leads to birefringence, with the dispersion relations of the ordinary and extraordinary rays given by $\omega^2/c^2 = (k_\parallel^2 + k_\perp^2)/\varepsilon_\perp$ and $\omega^2/c^2 = (k_\parallel^2/\varepsilon_\perp) + (k_\perp^2/\varepsilon_\parallel)$, respectively. The extraordinary rays have peculiar isofrequency open surfaces, shaped as single-sheet hyperboloids (*13–15*). When projected on the ω-$k_\perp$ plane, the hyperboloids fill a continuous region (orange fringes in Fig. 3E). The transverse $k_\parallel$ and axial $k_\perp$ momenta of these extraordinary polaritons can be very large, being limited only by the atomic structure of the material.

Polaritons can only propagate at angles θ or $\pi - \theta$ with respect to the optical axis satisfying the relation $\tan\theta = |\varepsilon_\perp/\varepsilon_\parallel|^{1/2}$. This implies that the polariton can be focused into narrow beams that do not spread laterally as they propagate through the material (see below). A thin slab with surfaces normal to the optical axis supports weakly confined surface modes that evolve into the principal branch of the guided waves as k increases (Fig. 3F). This is accompanied by numerous higher-order branches (Fig. 3F) that arise from splitting of the extraordinary ray continuum in Fig. 3E. The group velocity can be negative in a hyperbolic material, as demonstrated by direct imaging (*16*, *17*). Hyperbolic electrodynamics is ubiquitous in vdW materials and originates not only in the phonon modes (Fig. 3, E and F) but also in a highly anisotropic electronic response.

Plasmon-phonon polaritons are more complex modes involving the hybridization of the corresponding elemental excitations in heterostructures. For example, in graphene supported by hexagonal boron nitride (h-BN) (*18*, *60*) (Fig. 3E), the hyperbolic guided waves (*13–15*) appear in the two bands marked type I and type II. Outside these bands, one finds SPP and SP branches similar to those in Fig. 3B. The slope of the SP dispersion—the group velocity v_g—is much smaller than c: The light cone is nearly vertical (and hence invisible) in Fig. 3G. Additionally, v_g nearly everywhere exceeds the Fermi velocity and the plasmon does not overlap the electron-hole pair continuum (green region in Fig. 3G), so Landau damping is prevented.

New physics revealed by polaritonic observations

Polaritons in vdW materials provide unique opportunities for exploring electronic phenomena and lattice dynamics. In particular, polaritonic images grant us access into regions of the dispersion relations of various excitations beyond what is attainable with conventional optics.

Interactions and many-body effects

The decay rate and wavelength of plasmonic and polaritonic waves (Fig. 1) are determined by the complex optical conductivity $\sigma(k, \omega)$ of the medium that supports these waves. It is thus possible to reconstruct $\sigma(k, \omega)$ from polaritonic images, which contain information on both electronic and lattice dynamics (*10*, *19–21*). Specifically, the periodicity of plasmonic waves in graphene (Fig. 1A) is determined by the imaginary part of the conductivity, whereas the rate at which these waves decay into the interior of the samples is governed by Re σ/Im σ. The plasmon propagation length $\sim$(Im σ/Re σ)λ_p has been shown to reach $\sim$1 μm (i.e., tens of plasmon wavelengths) in
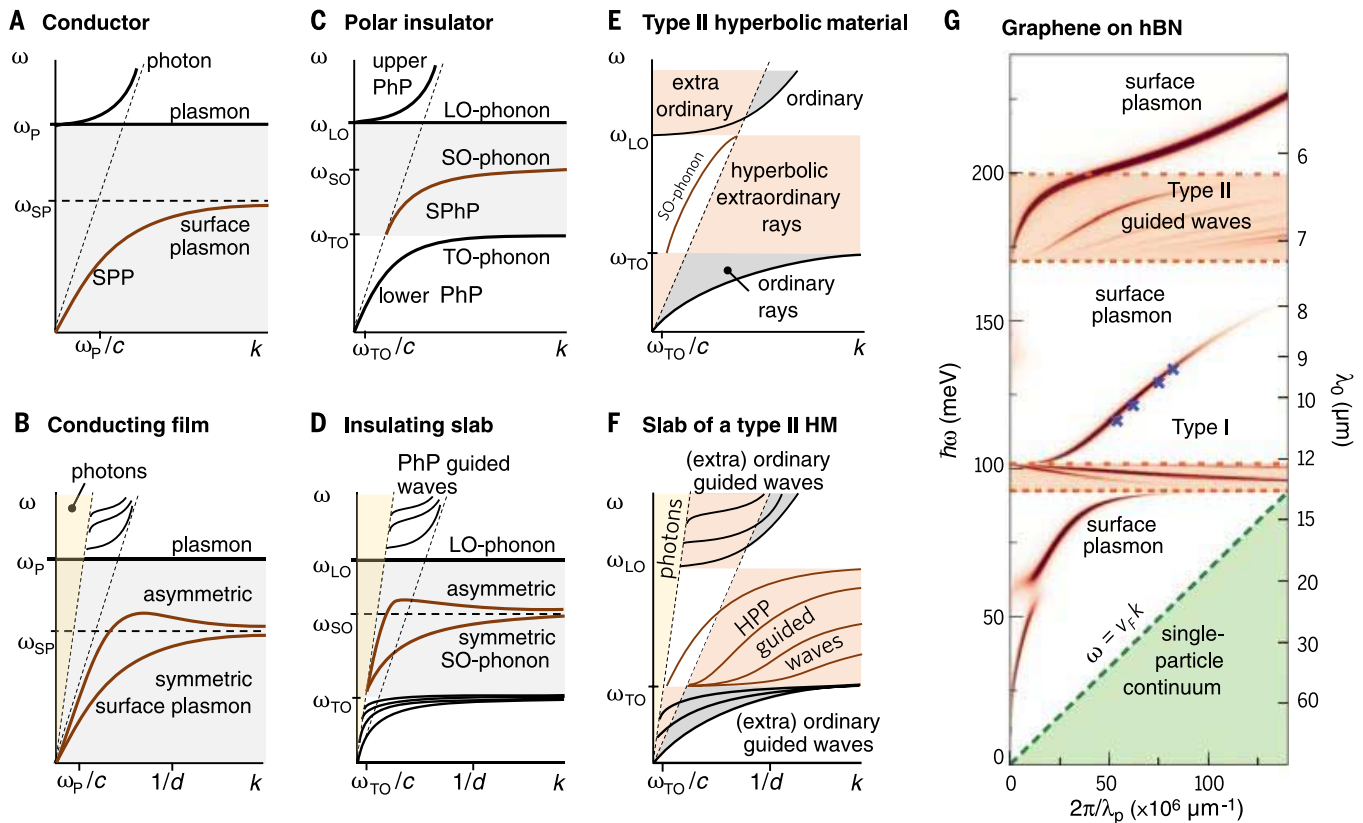
Fig. 3. Polariton dispersions. (**A**) Bulk conductors (metals or doped semiconductors). (**B**) Thin conducting films. (**C**) Isotropic polar dielectrics. (**D**) Thin polar dielectric slabs. (**E**) Type II hyperbolic materials. (**F**) Thin slab of a type II hyperbolic material with its optical axis normal to the surfaces. (**G**) Graphene–h-BN heterostructures (*10*). The horizontal axis is the transverse wave vector in (E) and the 3D bulk or in-plane wave vector in the other plots, depending on the mode. [Adapted from (*10*)]

high-mobility encapsulated graphene (*10*, *19*). The corresponding lifetime, ~500 fs, is only weakly dependent on gate voltage or probing photon frequency from the terahertz to mid-infrared regimes (*22*). This result is consistent with the dominant role of acoustic phonons in scattering processes (*9*), a conjecture further supported by theoretical analysis of the ω and k dependence of the plasmon scattering rate τ^{-1} = (Re σ/Im σ)ω (Fig. 4A). Data on interactions among electrons, phonons, and plasmons in other vdW systems are fragmentary, but implications of these interfacial effects may be quite spectacular. For example, coupling between electrons in monolayer FeSe and phonons in $SrTiO_3$ appears as a viable mechanism for high-temperature superconductivity in $FeSe/SrTiO_3$ heterostructures (*23*).

Polaritonic probe of the electronic structure and inhomogeneities

Equations 1 and 2 establish that images of polaritonic waves in a given medium encode the optical conductivity, and hence the fundamental information about intraband, interband, and excitonic effects within that medium. For example, the analysis of plasmonic reflections and standing waves has been used to decipher the electronic structure of moiré superlattices

formed at the interface of slightly mismatched hexagonal lattices of graphene and h-BN (*24*). Moiré patterns are periodic superlattice structures that appear when two crystals with a small lattice mismatch are superimposed. Moiré superlattices reveal the energy gap in the otherwise gapless electronic structure of graphene and therefore modify the conductivity σ(k, ω). The boundary between plain and superlattice graphene is thus associated with an abrupt change of the electronic conductivity—a property that prompts plasmonic reflections (Fig. 1D). The magnitude of the moiré-induced energy gap is inferred from a systematic analysis of these plasmonic patterns collected at different wavelengths for specimens with different doping. Plasmonic reflections also occur at other forms of electronic discontinuities, including grain boundaries in extended graphene films (*25*, *26*), stacking domains (Fig. 4C) in bilayer graphene (*27*), and nanometer-scale local gates (*28*, *29*). In particular, a carbon nanotube (CNT) gate acts as a perturbation produced by a line of charge, which introduces 1D-bound states in an adjacent graphene layer. In a related context, plasmons imaged in CNTs (Fig. 1C) are found to exhibit approximately doping- and frequency-independent (quantized) group velocity, which is a consequence of the 1D nature of these materials (*30*). We note

that 1D phonon polaritons are also observed in BN nanotubes (*31*).

Polaritons far and away from equilibrium

When subjected to photoexcitation by short and intense optical pulses, vdW polaritons can radically change their properties (*32*). Hyperspectral near-field imaging of graphene under intense optical pumping (*19*) (Fig. 4B) uncovers the emergence of mid-infrared plasmons in a specimen that shows no such modes in equilibrium because of its low Drude spectral weight S_f (Eq. 1). This effect is driven by thermal smearing of conduction electrons, which produces a boost in $S_f \propto k_B T$ (where k_B is the Boltzmann constant); the electron temperatures can be as high as T = 5000 K (*33*). Ultrafast heating of electrons and plasmons may realize a regime in which the dynamics of an approximately equal number of electrons and holes in graphene resembles the behavior of viscous liquids described by relativistic hydrodynamics (*34*, *35*). Several theoretical works have discussed plasmon amplification in vdW materials (*36*, *37*) under photoexcitation, followed by a recent experimental report (*38*). Apart from probing inherent nonlinearities of the materials (*39*), an experimental implementation of these ideas may uncover pathways for mitigating or eliminating
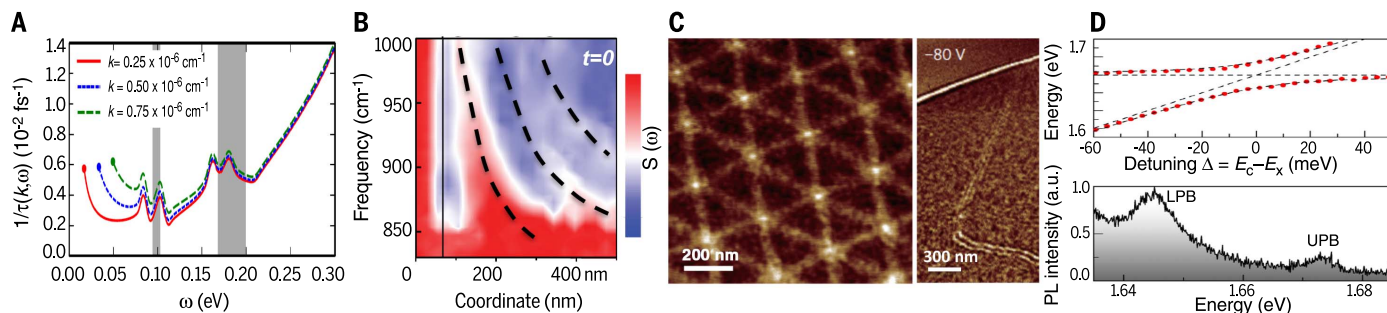
Fig. 4. Spectroscopy and imaging of polaritons enable a new line of inquiry into the fundamental physics of the media supporting polaritonic behavior. (A) Scattering rate $\tau^{-1}(k, \omega)$ for Dirac plasmons in monolayer graphene calculated (9) for three selected values of the in-plane wave vector k. Shaded areas correspond to stop bands. [Reproduced, with permission, from (9)] **(B)** Photoexcitation of semi-infinite monolayer graphene with intense femto-second pulses increases electronic temperature and enhances the spectral weight available for surface plasmons. Hyperspectral images (19) of the photoinduced change in the scattering amplitude $\Delta s(\omega, x)$ reveal the dispersion of photoinduced plasmons (red traces). A vertical line indicates the edge of the graphene sample. Dashed lines are theoretical fits. [Reproduced from (19)] **(C)** Nano-infrared contrast produced by plasmonic reflections at topological domain boundaries in bilayer graphene (27). [Reproduced, with permission, from (27)] **(D)** Exciton-photon coupling in a $MoSe_2$ double quantum-well hetero-structure showing an anticrossing between the neutral exciton and discrete cav-ity modes at 4.2 K. Top: A fit to the peak position as a function of detuning yields a Rabi splitting of 29 meV. Bottom: The upper and lower polariton branches (UPB and LPB) are well resolved spectrally (43). [Reproduced from (43)]

electronic losses in the plasmonic or polaritonic response. An alternative route for loss compensation consists of fulfilling the optical gain condition Re $\sigma(\omega) < 0$ by means of population inversion, an effect recently demonstrated (40) in the frequency range of excitonic transitions in WS_2.

High-temperature exciton polaritons

Atomically thin transition metal dichalcogenides (TMDs), including MoS_2 and $MoSe_2$, exhibit strong many-body effects due to their high effective carrier masses and low dielectric permittivities. Monolayers of TMDs are direct-gap semiconductors that host excitons with binding energies from 0.4 to 0.9 eV (41, 42). When integrated in an optical cavity, TMDs may form exciton polaritons, provided that the cavity-enhanced exciton-photon coupling (i.e., the Rabi frequency) exceeds the exciton decay rate (on the order of tens of meV). A realization of this regime was recently reported in a $MoSe_2$-based heterostructure (Fig. 4D) at 4.2 K (43) with a Rabi frequency of 29 meV and a clearly resolved avoided crossing of exciton and photon dispersions. Similar results were obtained for MoS_2 (44). The lower-k part of the exciton polariton–guided waves (Fig. 1F) has been imaged in thin WSe_2 crystals under ambient conditions (45), in a regime where these propagating modes have a dominant photon character (Fig. 1F).

A challenge for future nanoimaging experiments is to probe the strongly confined, large-k part of the exciton polariton branches. The exciton and exciton polariton propagation lengths are expected to be greatly enhanced if they form condensates, which are also predicted to occur in TMDs near room temperature (46), more than one order of magnitude higher than in conventional inorganic semiconductors. The interaction of exciton polariton condensates with a two-dimensional electron system of vdW materials may enable a new pathway toward high-temperature superconductivity (47, 48). Diverse polaritonic phenomena of excitonic origin may also be anticipated in CNTs, in view of the strong excitonic dipole activity of these 1D systems (49, 50).

Spatial dispersion

Nonlocal effects in the conductivity become relevant when the polariton wavelength is comparable with the Fermi wavelength λ_F. These phenomena remain largely unexplored in vdW materials. Nonlocal effects are typically investigated using momentum-resolved methods such as electron energy-loss spectroscopy, but they appear to be within reach for nano-optics techniques in view of the large values of λ_F in vdW layers. Nano-imaging and nanospectroscopy experiments allow one to determine the nonlocal conductivity (10, 51) $\sigma(k_P, \omega)$. Future nano-infrared measurements may provide additional insight into other momentum-dependent electronic phenomena (52).

Topological polaritonics

Topological order and Berry phases are playing a prominent role in the understanding of electronic properties of vdW solids such as chirality and anomalous Hall conductivity. These intriguing properties have implications in photonics and polaritonics (53, 54). For example, in gapped (bi-layer) graphene or TMDs, the anomalous Hall conductivities of the two valleys cancel each other in equilibrium. This cancellation can be removed through pumping with circularly polarized light, leading to a chiral polaritonic response (55, 56). Among many fascinating predictions exploring the roles of topology and chirality in polariton propagation, we mention those of chiral edge modes of plasmonic and excitonic origin (57). Recent observations of edge plasmons in graphene nanoribbons (Fig. 1B) fulfill the preconditions for exploring topological properties via polaritons.

Tailoring polaritonic characteristics specific to vdW materials

Stacking

Restacking of exfoliated and/or epitaxial vdW layers yields vertical heterostructures in which electromagnetic coupling between polaritonic modes of proximal planes gives rise to new optical properties beyond those of the individual constituents. For example, mid-infrared plasmons in graphene hybridize with phonon polaritons of an underlying polar substrate (18, 51, 58, 59). Hyperbolic polaritons observed in graphene–h-BN stacks (60) inherit electrostatic tunability from graphene and long propagation lengths from phonons in h-BN. Changes in electronic structure produced by interlayer interaction can further give rise to modified polaritonic response—for example, in rotationally aligned graphene–h-BN stacks, where the formation of long-period moiré superlattices modifies the dispersion and lifetime of composite plasmon polaritons (24). Finally, chiral twisted stacks may exhibit optical gyrotropy (61, 62).

Nanostructuring

Nanostructuring is commonly used to produce systems with reduced dimensionality, including stripes, discs, and nanocones of h-BN (63). Both artificial and natural boundaries of vdW samples harbor 1D polaritonic edge modes that reveal a dispersion distinct from that of "bulk" polaritons in the interior of vdW crystals (64, 65). Similarly, 1D modes are likely to occur at domain walls, lateral Josephson junctions, and p-n junctions.

Controls

Unlike conventional plasmonic media, vdW materials are amenable to active tuning of their polaritonic properties via chemical doping and gating. Graphene is a paramount example of this tunability. Additionally, doping of vdW semiconductors such as black phosphorus (66) affects the interplay between spectrally overlapping intra- and interband responses, which has an impact on their hyperbolic behavior (67). Persistent switching of optical properties can be realized in vdW/ferroelectric multilayers and by manipulating defects in h-BN layers (68). Optical pumping provides a mechanism of ultrafast control
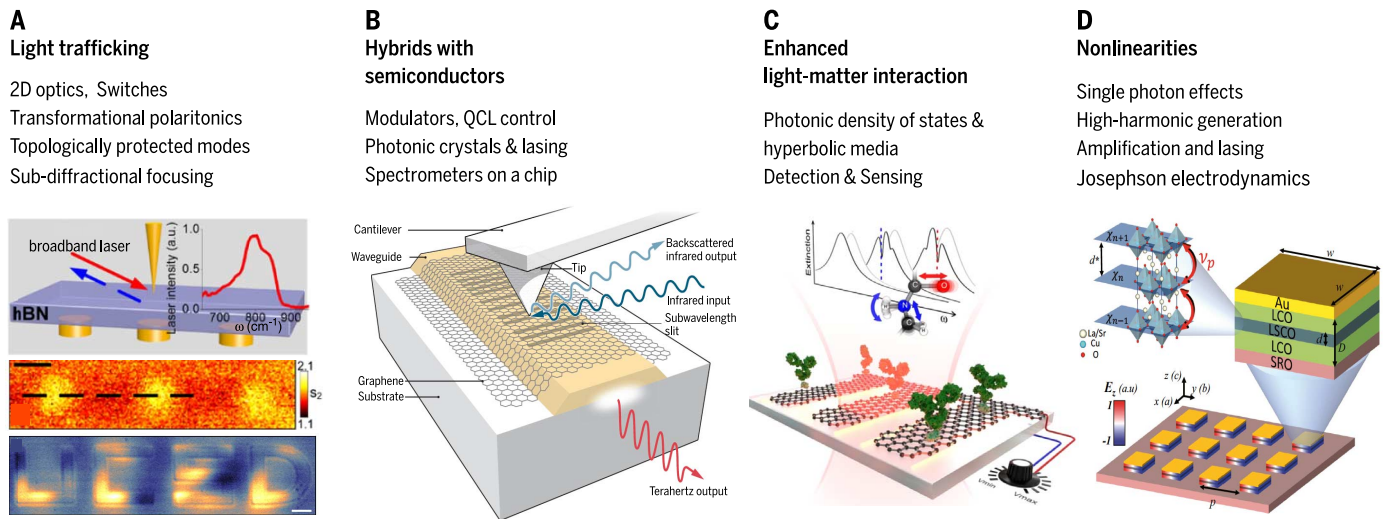
A
Light trafficking

2D optics, Switches
Transformational polaritonics
Topologically protected modes
Sub-diffractional focusing

B
Hybrids with semiconductors

Modulators, QCL control
Photonic crystals & lasing
Spectrometers on a chip

C
Enhanced light-matter interaction

Photonic density of states & hyperbolic media
Detection & Sensing

D
Nonlinearities

Single photon effects
High-harmonic generation
Amplification and lasing
Josephson electrodynamics

Fig. 5. Impending applications and future opportunities. (**A**) Subdiffractional focusing via phonon polaritons in h-BN ([16], [82]). Top: Au discs are deposited on the bottom surface of a h-BN slab. Middle: Image obtained on the top surface of the slab using a broadband source centered at $\lambda_O = 12.5$ μm; scale bar, 500 nm. Bottom: Image of a pattern showing subdiffractional features, acquired with $\lambda_O = 6$ μm; scale bar, 1 μm. [Reproduced from ([16], [82])] (**B**) Schematics of a quantum-cascade laser (QCL) with emission controlled by plasmons in the top graphene layer ([77], [78]). [Reproduced from ([78])] (**C**) Resonant absorption in graphene plasmonic strips for spectroscopic fingerprinting ([83]). [Reproduced from ([83])] (**D**) Proposed structure for investigating cavity electrodynamics of Josephson plasmons ([98]). LCO, La_2CuO_4; LSCO, $La_{2-x}Sr_xCuO_4$; SRO, $SrRuO_3$. [Reproduced, with permission, from ([98])]

([40], [69], [70]). Also, both strain and photoexcitation with circularly polarized light lift the valley degeneracy in vdW materials such as bilayer graphene and TMDs ([71]), enabling one to explore valley-selective phenomena. An expanding list of polaritonic "control knobs" includes population inversion ([40]), n- and p-type doping of graphene upon photoexcitation ([69]), magnetic fields applied to graphene ([72]), and strain engineering of excitons in WSe_2 ([73]).

Impending applications

The unusual optical properties displayed by vdW materials offer exciting opportunities for technological applications ([74]).

Light trafficking

Polariton nanoimaging experiments in vdW materials (Fig. 1) revealed that these ultracompact light-matter modes are capable of carrying optical signals over many micrometers in some cases. Furthermore, the propagation, reflection, and refraction of polaritons can be readily controlled by heterostructuring or through stimuli such as electrical gating ([20], [21]). Thus it is feasible to implement transformational polaritonics ([75]), polaritonic transistors, and integrated nanophotonic circuits using vdW systems. In heterostructures combining chiral and hyperbolic layers, it may be possible to produce polaritons topologically protected from backscattering, which could lead to protected unidirectional propagation and robustness against disorder ([53], [76]).

Electro-optical modulators

Integration of vdW materials with semiconductor photonics is equally appealing. Early demonstrations (Fig. 5B) include quantum-cascade lasers with tunable emission characteristics ([77], [78])

and electrically controlled modulators ([79]–[81]). The extreme reduction of the polariton wavelength in vdW materials should enable the design of ultrasmall spectrometers on a chip, with spectral resolution achieved through using different structures with polaritonic resonances covering a dense and broad set of frequencies.

Subdiffractional focusing and imaging

Compact but mobile phonon polaritons have already been used for subwavelength focusing and imaging (Fig. 5A), taking advantage of the hyperbolic dispersion of h-BN ([16], [82]). These properties could find application in detector arrays and lithographic imprinting at unprecedentedly small scales.

Optical sensing

Part of the success of metal-based plasmonics lies in its application to sensing, down to single molecules. This is made possible by exploiting the large concentration of electromagnetic energy associated with these optical modes. vdW polaritons produce even higher levels of field confinement than traditional plasmonic metals and therefore hold great potential for sensing. In particular, graphene-enabled ultrasensitive detection has recently been demonstrated for biological ([83]) and inorganic ([84]) molecules (Fig. 5C).

Light emission, amplification, and lasing

Spontaneous emission from a light-emitting device can be improved by coupling the radiated energy to polaritons ([2], [85]). This effect is particularly pronounced at the interface with hyperbolic media, where the photon density of states is greatly enhanced ([13]–[15]). The substantial field enhancement can also be used for efficient heat transfer at the nanoscale. Additionally, the low

saturation threshold of graphene has been exploited in fast mode-locked lasers ([86]), and polaritons in WSe_2 have recently been harnessed to implement an ultralow-threshold nanocavity laser ([87]).

Looking into the future

Polaritons in correlated van der Waals materials

Among the spectacular polaritonic effects intrinsic to vdW crystals, we highlight the Josephson plasmon originating from Cooper-pair tunneling between CuO_2 planes in layered cuprate high-T_c superconductors ([88]). Propagating and nonequilibrium Josephson plasmons are expected to provide insights ([89], [90]) into the unconventional superconductivity of these materials. Furthermore, the natural hyperbolic behaviors of cuprates, topological insulators ([14], [91]–[93]), and other anisotropic vdW compounds are yet to be exploited for imaging and focusing in a fashion similar to what has been done for h-BN (Fig. 5A).

Quantum and nonlinear optics with vdW polaritons

Decoherence is arguably the most serious impediment for a wide adoption of quantum technologies. The extreme concentration of electromagnetic energy associated with single polariton states in vdW materials can increase quantum interaction with neighboring optical emitters. Thus, it may be possible to reach the single-photon strong-coupling regime under ambient conditions, accompanied by nonlinearities down to the single-photon level ([94]). Notably, vdW materials exhibit unprecedented levels of nonlinearity, as revealed by wave-mixing experiments ([95]) as well as by harmonic-generation measurements ([96]), which are predicted to be boosted

by polaritonic field enhancement ([97]). Further explorations of nonlinear effects in vdW high-T_c superconductors may enable manipulation of the superconducting order parameter and phase coherence under nonequilibrium conditions ([98]). Strongly confined plasmonic modes in vdW materials may lead to increased rates of high-order multipolar transitions, two-plasmon spontaneous emission, and spin-flip transitions ([99]).

The study of polaritons in vdW materials is a vibrant area of research at the vanguard of physics, materials science, and engineering. Heterostructuring of atomic vdW layers, in conjunction with the inherent sensitivity of this class of materials to external stimuli, has uncovered opportunities for on-demand photonic and polaritonic characteristics. Novel visualization techniques have revealed the rich physics of vdW layers encoded in observed images of polaritonic waves. Nanoscale near-field imaging of polaritons is emerging as an experimental method providing new insights into quantum phenomena not attainable with conventional spectroscopies. Given the omnipresence of polaritons in condensed-matter systems, we anticipate this line of inquiry to continue to unfold novel effects in other classes of quantum materials.

REFERENCES AND NOTES

1. J. M. Atkin, S. Berweger, A. C. Jones, M. B. Raschke, Nano-optical imaging and spectroscopy of order, phases, and domains in complex solids. *Adv. Phys.* **61**, 745–842 (2012). doi: 10.1080/00018732.2012.737982

2. J. A. Schuller et al., Plasmonics for extreme light concentration and manipulation. *Nat. Mater.* **9**, 193–204 (2010). doi: 10.1038/nmat2630; pmid: 20168343

3. G. V. Naik, V. M. Shalaev, A. Boltasseva, Alternative plasmonic materials: Beyond gold and silver. *Adv. Mater.* **25**, 3264–3294 (2013). doi: 10.1002/adma.201205076

4. A. Boltasseva, H. A. Atwater, Low-loss plasmonic metamaterials. *Science* **331**, 290–291 (2011). doi: 10.1126/science.1198258; pmid: 21252335

5. P. Alonso-González et al., Controlling graphene plasmons with resonant metal antennas and spatial conductivity patterns. *Science* **344**, 1369–1373 (2014). doi: 10.1126/science.1253202; pmid: 24855026

6. F. J. García de Abajo, Optical excitations in electron microscopy. *Rev. Mod. Phys.* **82**, 209–275 (2010). doi: 10.1103/RevModPhys.82.209

7. S. Das Sarma, S. Adam, E. H. Hwang, E. Rossi, Electronic transport in two-dimensional graphene. *Rev. Mod. Phys.* **83**, 407–470 (2011). doi: 10.1103/RevModPhys.83.407

8. M. Jablan, H. Buljan, M. Soljačić, Plasmonics in graphene at infrared frequencies. *Phys. Rev. B* **80**, 245435 (2009). doi: 10.1103/PhysRevB.80.245435

9. A. Principi et al., Plasmon losses due to electron-phonon scattering: The case of graphene encapsulated in hexagonal boron nitride. *Phys. Rev. B* **90**, 165408 (2014). doi: 10.1103/PhysRevB.90.165408

10. A. Woessner et al., Highly confined low-loss plasmons in graphene-boron nitride heterostructures. *Nat. Mater.* **14**, 421–425 (2015). doi: 10.1038/nmat4169; pmid: 25532073

11. A. V. Zayats, I. I. Smolyaninov, A. A. Maradudin, Nano-optics of surface plasmon polaritons. *Phys. Rep.* **408**, 131–314 (2005). doi: 10.1016/j.physrep.2004.11.001

12. J. D. Caldwell et al., Low-loss, infrared and terahertz nanophotonics using surface phonon polaritons. *Nanophotonics* **4**, 44 (2015). doi: 10.1515/nanoph-2014-0003

13. A. Poddubny, I. Iorsh, P. Belov, Y. Kivshar, Hyperbolic metamaterials. *Nat. Photonics* **7**, 948–957 (2013). doi: 10.1038/nphoton.2013.243

14. J. Sun, N. M. Litchinitser, J. Zhou, Indefinite by nature: From ultraviolet to terahertz. *ACS Photonics* **1**, 293–303 (2014). doi: 10.1021/ph4000983

15. J. Kim et al., Improving the radiative decay rate for dye molecules with hyperbolic metamaterials. *Opt. Express* **20**, 8100–8116 (2012). doi: 10.1364/OE.20.008100; pmid: 22453481

16. S. Dai et al., Subdiffractional focusing and guiding of polaritonic rays in a natural hyperbolic material. *Nat. Commun.* **6**, 6963 (2015). doi: 10.1038/ncomms7963; pmid: 25902364

17. E. Yoxall et al., Direct observation of ultraslow hyperbolic polariton propagation with negative phase velocity. *Nat. Photonics* **9**, 674–678 (2015). doi: 10.1038/nphoton.2015.166

18. V. W. Brar et al., Hybrid surface-phonon-plasmon polariton modes in graphene/monolayer h-BN heterostructures. *Nano Lett.* **14**, 3876–3880 (2014). doi: 10.1021/nl501096s; pmid: 24874205

19. G. X. Ni et al., Ultrafast optical switching of infrared plasmon polaritons in high-mobility graphene. *Nat. Photonics* **10**, 244–247 (2016). doi: 10.1038/nphoton.2016.45

20. J. Chen et al., Optical nano-imaging of gate-tunable graphene plasmons. *Nature* **487**, 77–81 (2012). doi: 10.1038/nature11254; pmid: 22722861

21. Z. Fei et al., Gate-tuning of graphene plasmons revealed by infrared nano-imaging. *Nature* **487**, 82–85 (2012). doi: 10.1038/nature11253; pmid: 22722866

22. P. Alonso-Gonzalez et al., http://arxiv.org/abs/1601.05753 (2016).

23. J. J. Lee et al., Interfacial mode coupling as the origin of the enhancement of T_c in FeSe films on SrTiO₃. *Nature* **515**, 245–248 (2014). doi: 10.1038/nature13894; pmid: 25391962

24. G. X. Ni et al., Plasmons in graphene moiré superlattices. *Nat. Mater.* **14**, 1217–1222 (2015). doi: 10.1038/nmat4425; pmid: 26413987

25. Z. Fei et al., Electronic and plasmonic phenomena at graphene grain boundaries. *Nat. Nanotechnol.* **8**, 821–825 (2013). doi: 10.1038/nnano.2013.197; pmid: 24122082

26. J. Chen et al., Strong plasmon reflection at nanometer-size gaps in monolayer graphene on SiC. *Nano Lett.* **13**, 6210–6215 (2013). doi: 10.1021/nl403622t; pmid: 24188400

27. L. Jiang et al., Soliton-dependent plasmon reflection at bilayer graphene domain walls. *Nat. Mater.* **15**, 840–844 (2016). doi: 10.1038/nmat4653

28. A. Woessner et al., Near-field photocurrent nanoscopy on bare and encapsulated graphene. *Nat. Commun.* **7**, 10783 (2016). doi: 10.1038/ncomms10783; pmid: 26916951

29. B.-Y. Jiang et al., Tunable plasmonic reflection by bound 1D electron states in a 2D Dirac metal. *Phys. Rev. Lett.* **117**, 086801 (2016). doi: 10.1103/PhysRevLett.117.086801

30. Z. Shi et al., Observation of a Luttinger-liquid plasmon in metallic single-walled carbon nanotubes. *Nat. Photonics* **9**, 515–519 (2015). doi: 10.1038/nphoton.2015.123

31. X. G. Xu, A. E. Tanur, G. C. Walker, Phase controlled homodyne infrared near-field microscopy and spectroscopy reveal inhomogeneity within and among individual boron nitride nanotubes. *J. Phys. Chem.* **117**, 3348–3354 (2013). doi: 10.1021/jp4008784

32. F. J. García de Abajo, Graphene nanophotonics: Challenges and opportunities. *ACS Photonics* **1**, 135–152 (2014). doi: 10.1021/ph400147y

33. M. Wagner et al., Ultrafast and nanoscale plasmonic phenomena in exfoliated graphene revealed by infrared pump-probe nanoscopy. *Nano Lett.* **14**, 894–900 (2014). doi: 10.1021/nl4042577; pmid: 24479682

34. D. A. Bandurin et al., Negative local resistance caused by viscous electron backflow in graphene. *Science* **351**, 1055–1058 (2016). doi: 10.1126/science.aad0201; pmid: 26912363

35. J. Crossno et al., Observation of the Dirac fluid and the breakdown of the Wiedemann-Franz law in graphene. *Science* **351**, 1058–1061 (2016). doi: 10.1126/science.aad0343; pmid: 26912162

36. F. F. Rana, Graphene terahertz plasmon oscillators. *IEEE Trans. Nanotechnol.* **7**, 91–99 (2008). doi: 10.1109/TNANO.2007.910334

37. Z. Sun, D. N. Basov, M. M. Fogler, Adiabatic amplification of plasmons and demons in 2D systems. *Phys. Rev. Lett.* **117**, 076805 (2016). doi: 10.1103/PhysRevLett.117.076805

38. S. Rajasekaran et al., Parametric amplification of a superconducting plasma wave. *Nat. Phys.* 10.1038/NPhys3819 (2016). doi: 10.1038/NPhys3819

39. J. B. Khurgin, Graphene—A rather ordinary nonlinear optical material. *Appl. Phys. Lett.* **104**, 161116 (2014). doi: 10.1063/1.4873704

40. A. Chernikov, C. Ruppert, H. M. Hill, A. F. Rigosi, T. F. Heinz, Population inversion and giant bandgap renormalization in atomically thin WS₂ layers. *Nat. Photonics* **9**, 466–470 (2015). doi: 10.1038/nphoton.2015.104

41. F. Xia, H. Wang, D. Xiao, M. Dubey, A. Ramasubramaniam, Two-dimensional material nanophotonics. *Nat. Photonics* **8**, 899–907 (2014). doi: 10.1038/nphoton.2014.271

42. K. F. Mak, C. Lee, J. Hone, J. Shan, T. F. Heinz, Atomically thin MoS₂: A new direct-gap semiconductor. *Phys. Rev. Lett.* **105**, 136805 (2010). doi: 10.1103/PhysRevLett.105.136805; pmid: 21230799

43. S. Dufferwiel et al., Exciton-polaritons in van der Waals heterostructures embedded in tunable microcavities. *Nat. Commun.* **6**, 8579 (2015). doi: 10.1038/ncomms9579

44. X. Liu et al., Strong light-matter coupling in two-dimensional atomic crystals. *Nat. Photonics* **9**, 30–34 (2015). doi: 10.1038/nphoton.2014.304

45. Z. Fei et al., Nano-optical imaging of WS e₂ waveguide modes revealing light-exciton interactions. *Phys. Rev. B* **94**, 081402(R) (2016). doi: 10.1103/PhysRevB.94.081402

46. M. M. Fogler, L. V. Butov, K. S. Novoselov, High-temperature superfluidity with indirect excitons in van der Waals heterostructures. *Nat. Commun.* **5**, 4555 (2014). doi: 10.1038/ncomms5555; pmid: 25065343

47. F. P. Laussy, A. V. Kavokin, I. A. Shelykh, Exciton polariton mediated superconductivity. *Phys. Rev. Lett.* **104**, 106402 (2010). doi: 10.1103/PhysRevLett.104.106402

48. O. Cotlet, S. Zeytinoglu, M. Sigrist, E. Demler, A. Imamoglu, Superconductivity and other collective phenomena in a hybrid Bose-Fermi mixture formed by a polariton condensate and an electron system in two dimensions. *Phys. Rev. B* **93**, 054510 (2016). doi: 10.1103/PhysRevB.93.054510

49. F. Wang, G. Dukovic, L. E. Brus, T. F. Heinz, The optical resonances in carbon nanotubes arise from excitons. *Science* **308**, 838–841 (2005). doi: 10.1126/science.1110265; pmid: 15879212

50. I. V. Bondarev, L. M. Woods, K. Tatur, Strong exciton-plasmon coupling in semiconducting carbon nanotubes. *Phys. Rev. B* **80**, 085407 (2009). doi: 10.1103/PhysRevB.80.085407

51. Z. Fei et al., Infrared nanoscopy of Dirac plasmons at the graphene-SiO₂ interface. *Nano Lett.* **11**, 4701–4705 (2011). doi: 10.1021/nl202362d; pmid: 21972938

52. J. P. Carbotte, J. P. F. LeBlanc, E. J. Nicol, Emergence of plasmaronic structure in the near-field optical response of graphene. *Phys. Rev. B* **85**, 201411(R) (2012). doi: 10.1103/PhysRevB.85.201411

53. L. Lu, J. D. Joannopoulos, M. Soljačić, Topological photonics. *Nat. Photonics* **8**, 821–829 (2014). doi: 10.1038/nphoton.2014.248

54. K. Y. Bliokh, F. J. Rodríguez-Fortuño, F. Nori, A. V. Zayats, Spin-orbit interactions of light. *Nat. Photonics* **9**, 796–808 (2015). doi: 10.1038/nphoton.2015.201

55. J. C. W. Song, M. S. Rudner, Chiral plasmons without magnetic field. *Proc. Natl. Acad. Sci. U.S.A.* **113**, 4658–4663 (2016). doi: 10.1073/pnas.1519086113; pmid: 27071090

56. A. Kumar et al., Chiral plasmon in gapped Dirac systems. *Phys. Rev. B* **93**, 041413(R) (2016). doi: 10.1103/PhysRevB.93.041413

57. T. Karzig, C.-E. Bardyn, N. H. Lindner, G. Refael, Topological polaritons. *Phys. Rev. X* **5**, 031001 (2015). doi: 10.1103/PhysRevX.5.031001

58. A. Kumar, T. Low, K. H. Fung, P. Avouris, N. X. Fang, Tunable light-matter interaction and the role of hyperbolicity in graphene-hBN system. *Nano Lett.* **15**, 3172–3180 (2015). doi: 10.1021/acs.nanolett.5b01191; pmid: 25897983

59. J. D. Caldwell et al., Atomic-scale photonic hybrids for mid-infrared and terahertz nanophotonics. *Nat. Nanotechnol.* **11**, 9–15 (2016). doi: 10.1038/nnano.2015.305

60. S. Dai et al., Graphene on hexagonal boron nitride as a tunable hyperbolic metamaterial. *Nat. Nanotechnol.* **10**, 682–686 (2015). doi: 10.1038/nnano.2015.131; pmid: 26098228

61. C.-J. Kim et al., Chiral atomically thin films. *Nat. Nanotechnol.* **11**, 520–524 (2016). doi: 10.1038/nnano.2016.3; pmid: 26900756

62. P.-C. Yeh et al., Direct measurement of the tunable electronic structure of bilayer MoS₂ by interlayer twist. *Nano Lett.* **16**, 953–959 (2016). doi: 10.1021/acs.nanolett.5b03883; pmid: 26760447

63. A. J. Giles et al., Imaging of anomalous internal reflections of hyperbolic phonon-polaritons in hexagonal boron nitride. *Nano Lett.* **16**, 3858–3865 (2016). doi: 10.1021/acs.nanolett.6b01341

64. Z. Fei et al., Edge and surface plasmons in graphene nanoribbons. *Nano Lett.* **15**, 8271–8276 (2015). doi: 10.1021/acs.nanolett.5b03834; pmid: 26571096

65. A. Y. Nikitin et al., Real-space mapping of tailored sheet and edge plasmons in graphene nanoresonators. Nat. Photonics 10, 239–243 (2016). doi: 10.1038/nphoton.2016.44

66. S. Gamage et al., Nanoscopy of black phosphorus degradation. Adv. Mater. Interfaces 10.1002/admi.201600121 (2016). doi: 10.1002/admi.201600121

67. A. Nemilentsau, T. Low, G. Hanson, Anisotropic 2D materials for tunable hyperbolic plasmonics. Phys. Rev. Lett. 116, 066804 (2016). doi: 10.1103/PhysRevLett.116.066804; pmid: 26919007

68. J. Velasco Jr. et al., Nanoscale control of rewriteable doping patterns in pristine graphene/boron nitride heterostructures. Nano Lett. 16, 1620–1625 (2016). doi: 10.1021/acs.nanolett.5b04441; pmid: 26852622

69. Z. Fang et al., Plasmon-induced doping of graphene. ACS Nano 6, 10222–10228 (2012). doi: 10.1021/nn304028b; pmid: 22998468

70. F. H. L. Koppens et al., Photodetectors based on graphene, other two-dimensional materials and hybrid systems. Nat. Nanotechnol. 9, 780–793 (2014). doi: 10.1038/nnano.2014.215; pmid: 25286273

71. X. Xu, W. Yao, D. Xiao, T. F. Heinz, Spin and pseudospins in layered transition metal dichalcogenides. Nat. Phys. 10, 343–350 (2014). doi: 10.1038/nphys2942

72. I. Crassee et al., Intrinsic terahertz plasmons and magnetoplasmons in large scale monolayer graphene. Nano Lett. 12, 2470–2474 (2012). doi: 10.1021/nl300572y; pmid: 22519967

73. K.-D. Park et al., Hybrid tip-enhanced nanospectroscopy and nanoimaging of monolayer WSe$_2$ with local strain control. Nano Lett. 16, 2621–2627 (2016). doi: 10.1021/acs.nanolett.6b00238

74. P. Bharadwaj, L. Novotny, Optoelectronics in Flatland. Opt. Photon. News 26, 24 (2015). doi: 10.1364/OPN.26.7.000024

75. A. Vakil, N. Engheta, Transformation optics using graphene. Science 332, 1291–1294 (2011). doi: 10.1126/science.1202691; pmid: 21659598

76. W. Gao et al., Topological photonic phase in chiral hyperbolic metamaterials. Phys. Rev. Lett. 114, 037402 (2015). doi: 10.1103/PhysRevLett.114.037402; pmid: 25659022

77. S. Chakraborty et al., Gain modulation by graphene plasmons in aperiodic lattice lasers. Science 351, 246–248 (2016). doi: 10.1126/science.aad2930; pmid: 26816373

78. M. Polini, Tuning terahertz lasers via graphene plasmons. Science 351, 229–231 (2016). doi: 10.1126/science.aad7995; pmid: 26816365

79. Z. Fang et al., Gated tunability and hybridization of localized plasmons in nanostructured graphene. ACS Nano 7, 2388–2395 (2013). doi: 10.1021/nn3055835; pmid: 23390960

80. M. Liu et al., A graphene-based broadband optical modulator. Nature 474, 64–67 (2011). doi: 10.1038/nature10067; pmid: 21552277

81. C. T. Phare, Y.-H. D. Lee, J. Cardenas, M. Lipson, Graphene electro-optic modulator with 30 GHz bandwidth. Nat. Photonics 9, 511–514 (2015). doi: 10.1038/nphoton.2015.122

82. P. Li et al., Hyperbolic phonon-polaritons in boron nitride for near-field optical imaging and focusing. Nat. Commun. 6, 7507 (2015). doi: 10.1038/ncomms8507; pmid: 26112474

83. D. Rodrigo et al., Mid-infrared plasmonic biosensing with graphene. Science 349, 165–168 (2015). doi: 10.1126/science.aab2051; pmid: 26160941

84. D. B. Farmer, P. Avouris, Y. Li, T. F. Heinz, S.-J. Han, Ultrasensitive plasmonic detection of molecules with graphene. ACS Photonics 3, 553–557 (2016). doi: 10.1021/acsphotonics.6b00143

85. J. B. Khurgin, G. Sun, R. A. Soref, Enhancement of luminescence efficiency using surface plasmon polaritons: Figures of merit. J. Opt. Soc. Am. B 24, 1968 (2007). doi: 10.1364/JOSAB.24.001968

86. T. Hasan et al., Nanotube-polymer composites for ultrafast photonics. Adv. Mater. 21, 3874–3899 (2009). doi: 10.1002/adma.200901122

87. S. Wu et al., Monolayer semiconductor nanocavity lasers with ultralow thresholds. Nature 520, 69–72 (2015). doi: 10.1038/nature14290; pmid: 25778703

88. D. N. Basov, T. Timusk, Electrodynamics of high-T$_c$ superconductors. Rev. Mod. Phys. 77, 721–779 (2005). doi: 10.1103/RevModPhys.77.721

89. H. T. Stinson et al., Infrared nanospectroscopy and imaging of collective superfluid excitations in anisotropic superconductors. Phys. Rev. B 90, 014502 (2014). doi: 10.1103/PhysRevB.90.014502

90. A. Tsiatmas, V. A. Fedotov, F. J. García de Abajo, N. I. Zheludev, Low-loss terahertz superconducting plasmonics. New J. Phys. 14, 115006 (2012). doi: 10.1088/1367-2630/14/11/115006

91. E. E. Narimanov, A. V. Kildishev, Metamaterials: Naturally hyperbolic. Nat. Photonics 9, 214–216 (2015). doi: 10.1038/nphoton.2015.56

92. J. B. Khurgin, Two-dimensional exciton-polariton—light guiding by transition metal dichalcogenide monolayers. Optica 2, 740 (2015). doi: 10.1364/OPTICA.2.000740

93. J.-S. Wu, D. N. Basov, M. M. Fogler, Topological insulators are tunable waveguides for hyperbolic polaritons. Phys. Rev. B 92, 205430 (2015). doi: 10.1103/PhysRevB.92.205430

94. M. Gullans, D. E. Chang, F. H. L. Koppens, F. J. García de Abajo, M. D. Lukin, Single-photon nonlinear optics with graphene plasmons. Phys. Rev. Lett. 111, 247401 (2013). doi: 10.1103/PhysRevLett.111.247401; pmid: 24483697

95. T. J. Constant, S. M. Hornett, D. E. Chang, E. Hendry, All-optical generation of surface plasmons in graphene. Nat. Phys. 12, 124–127 (2016). doi: 10.1038/nphys3545

96. X. Yin et al., Edge nonlinear optics on a MoS$_2$ atomic monolayer. Science 344, 488–490 (2014). doi: 10.1126/science.1250564; pmid: 24786072

97. J. D. Cox, F. Javier García de Abajo, Electrically tunable nonlinear plasmonics in graphene nanoislands. Nat. Commun. 5, 5725 (2014). doi: 10.1038/ncomms6725; pmid: 25500534

98. Y. Laplace, S. Fernandez-Pena, S. Gariglio, J. M. Triscone, A. Cavalleri, Proposed cavity Josephson plasmonics with complex-oxide heterostructures. Phys. Rev. B 93, 075152 (2016). doi: 10.1103/PhysRevB.93.075152

99. N. Rivera, I. Kaminer, B. Zhen, J. D. Joannopoulos, M. Soljačić, Shrinking light to allow forbidden transitions on the atomic scale. Science 353, 263–269 (2016). doi: 10.1126/science.1250564; pmid: 24786072

100. J. A. Gerber, S. Berweger, B. T. O'Callahan, M. B. Raschke, Phase-resolved surface plasmon interferometry of graphene. Phys. Rev. Lett. 113, 055502 (2014). doi: 10.1103/PhysRevLett.113.055502; pmid: 25126927

101. A. Tomadin, F. Guinea, M. Polini, Generation and morphing of plasmons in graphene superlattices. Phys. Rev. B 90, 161406(R) (2014). doi: 10.1103/PhysRevB.90.161406

102. S. Dai et al., Tunable phonon polaritons in atomically thin van der Waals crystals of boron nitride. Science 343, 1125–1129 (2014). doi: 10.1126/science.1246833; pmid: 24604197

103. J. D. Caldwell et al., Sub-diffractional volume-confined polaritons in the natural hyperbolic material hexagonal boron nitride. Nat. Commun. 5, 5221 (2014). doi: 10.1038/ncomms6221; pmid: 25323633

104. Z. Shi et al., Amplitude- and phase-resolved nanospectral imaging of phonon polaritons in hexagonal boron nitride. ACS Photonics 2, 790–796 (2015). doi: 10.1021/acsphotonics.5b00007

105. A. Politano et al., Interplay of surface and Dirac plasmons in topological insulators: The case of Bi$_2$Se$_3$. Phys. Rev. Lett. 115, 216802 (2015). doi: 10.1103/PhysRevLett.115.216802; pmid: 26636863

106. A. Kogar et al., Surface collective modes in the topological insulators Bi$_2$Se$_3$ and Bi$_{0.5}$Sb$_{1.5}$Te$_{3-x}$Se$_x$. Phys. Rev. Lett. 115, 257402 (2015). doi: 10.1103/PhysRevLett.115.257402; pmid: 26722943

107. V. A. Golick et al., Surface Josephson plasma waves in layered superconductors above the plasma frequency: Evidence for a negative index of refraction. Phys. Rev. Lett. 104, 187003 (2010). doi: 10.1103/PhysRevLett.104.187003; pmid: 20482202

108. F. J. Dunmore, D. Z. Liu, H. D. Drew, S. Das Sarma, Observation of below-gap plasmon excitations in superconducting YBa$_2$Cu$_3$O$_7$ films. Phys. Rev. B 52, R731(R) (1995). doi: 10.1103/PhysRevB.R731; pmid:9980738

109. T. Low et al., Plasmons and screening in monolayer and multilayer black phosphorus. Phys. Rev. Lett. 113, 106802 (2014). doi: 10.1103/PhysRevLett.113.106802; pmid: 25238376

110. H. Yan et al., Damping pathways of mid-infrared plasmons in graphene nanostructures. Nat. Photonics 7, 394–399 (2013). doi: 10.1038/nphoton.2013.57

111. L. Ju et al., Graphene plasmonics for tunable terahertz metamaterials. Nat. Nanotechnol. 6, 630–634 (2011). doi: 10.1038/nnano.2011.146; pmid: 21892164

112. M. Autore et al., Plasmon-phonon interactions in topological insulator microrings. Adv. Opt. Mater. 3, 1257–1263 (2015). doi: 10.1002/adom.201400513

113. F. J. García de Abajo, Multiple excitation of confined graphene plasmons by single free electrons. ACS Nano 7, 11409–11419 (2013). doi: 10.1021/nn405367e; pmid: 24219514

114. F. H. L. Koppens, D. E. Chang, F. J. García de Abajo, Graphene plasmonics: A platform for strong light-matter interactions. Nano Lett. 11, 3370–3377 (2011). doi: 10.1021/nl201771h; pmid: 21766812

115. A. Yu. Nikitin, F. Guinea, F. J. Garcia-Vidal, L. Martin-Moreno, Fields radiated by a nanoemitter in a graphene sheet. Phys. Rev. B 84, 195446 (2011). doi: 10.1103/PhysRevB.84.195446

116. R. Beams, P. Bharadwaj, L. Novotny, Electroluminescence from graphene excited by electron tunneling. Nanotechnology 25, 055206 (2014). doi: 10.1088/0957-4484/25/5/055206; pmid: 24407020

117. J. Schiefele, J. Pedrós, F. Sols, F. Calle, F. Guinea, Coupling light into graphene plasmons through surface acoustic waves. Phys. Rev. Lett. 111, 237405 (2013). doi: 10.1103/PhysRevLett.111.237405; pmid: 24476304

118. M. Farhat, S. Guenneau, H. Bagci, Exciting graphene surface plasmon polaritons through light and sound interplay. Phys. Rev. Lett. 111, 237404 (2013). doi: 10.1103/PhysRevLett.111.237404